Article

Study on Motion Response Prediction of Offshore Platform Based on Multi-Sea State Samples and EMD Algorithm

Tianyu Liu [1,2], Feng Diao [1,3], Wen Yao [1], Franck Aurel Likeufack Mdemaya [2] and Gang Xu [2,4,*]

[1] Taihu Laboratory of Deepsea Technological Science Lianyungang Center, Lianyungang 222000, China; 18905218536@163.com (T.L.); diaofeng@702sh.com (F.D.); edwin_yao@163.com (W.Y.)

[2] School of Naval Architecture and Ocean Engineering, Jiangsu University of Science and Technology, Zhenjiang 212100, China; mdemayaaurel@yahoo.fr

[3] China Ship Scientific Research Center, Wuxi 214082, China

[4] Marine Equipment and Technology Institute, Jiangsu University of Science and Technology, Zhenjiang 212100, China

[*] Correspondence: g.xu@just.edu.cn; Tel.: +86-0511-15189100515

Abstract: The complexity of offshore operations demands that offshore platforms withstand the variability and uncertainty of marine environments. Consequently, analyses of platform motion responses must extend beyond single sea state conditions. This study employs the Computational Fluid Dynamics (CFDs) software STAR-CCM+ for data acquisition and investigates platform motion from two perspectives: adaptability analysis to different wave directions and adaptability analysis to varying significant wave heights. The aim is to develop a model capable of predicting offshore platform motion responses across multiple sea state conditions. The results demonstrate that integrating the empirical mode decomposition (EMD) algorithm with residual convolutional neural networks (ResCNNs) and Long Short-Term Memory (LSTM) networks effectively resolves the challenge of insufficient prediction accuracy under diverse maritime conditions. Following EMD incorporation, the model's performance within the predictive range was significantly enhanced, with the coefficient of determination (R^2) consistently exceeding 0.5, indicating a high degree of model fit to the data. Concurrently, the mean squared error (MSE) and Mean Absolute Percentage Error (MAPE) metrics exhibited commendable performance, further substantiating the model's precision and reliability. This methodology introduces an innovative approach for forecasting the dynamic responses of offshore structures, providing a more rigorous and accurate foundation for maritime operational decisions. Ultimately, the research enhances the safety and productivity of offshore activities.

Keywords: neural networks; EMD; offshore platform; motion response; sea state condition

1. Introduction

In ocean engineering, accurately predicting the motion of offshore platforms under varying sea state conditions is crucial for their offshore operations. The precise prediction of offshore platform motion is of paramount importance for maintaining operational safety, enhancing efficiency, and reducing costs in the field of marine engineering. Accurate forecasting significantly mitigates the risks of platform capsizing and collisions due to changes in sea conditions, thereby safeguarding the lives of personnel and the integrity of equipment. Furthermore, it enables operators to plan offshore operations more effectively, optimize operational processes, and thereby increase operational efficiency [1]. Concurrently, accurate predictions help to minimize equipment damage caused by adverse sea conditions, significantly reducing the economic costs associated with offshore operations. The synergistic effect of these factors not only improves the economic benefits of offshore operations but also actively promotes the sustainable development and utilization of marine resources. The marine environment's inherent complexity and uncertainty have historically made platform motion prediction challenging. However, advancements in computing

technology and data acquisition have transformed this domain, with Computational Fluid Dynamics (CFDs) and neural network technologies emerging as prominent research areas. Marine modeling and ship motion prediction have improved with advanced machine learning and hybrid models. Jae-Hoon Lee [2] has investigated an artificial neural network system for ship motion prediction in navigation channels, integrating a neural network based on Long Short-Term Memory (LSTM) encoders and decoders with convolutional neural networks (CNNs) to account for the physical characteristics of ship motion induced by waves. Chang-Zhe Chen [3] proposed a novel reduced-order model (ROM) based on high-order dynamic mode decomposition (HODMD) for time-series prediction of ship heading-keeping motion in waves. Elkhrachy [4] applied the Sverdrup Munk Bretschneider (SMB) semi-analytical approach, along with the Emotional Artificial Neural Network (EANN) and Wavelet Artificial Neural Network (WANN), to estimate wave characteristics in the Gulf of Mexico and the Aleutian Basin. This research endeavored to assess the precision and reliability of these methodologies and to scrutinize the variations in wave patterns across different spaces and times. Heydarizad M [5] proposed a novel model based on artificial neural networks (ANNs), stepwise regression, and ensemble machine learning methods to simulate the stable isotope characteristics in precipitation. Jinxiu Zhao [6] introduces a fully adaptive model for time–frequency coupling forecasting, which is grounded in the Deep Operator Network and incorporates a self-attention mechanism. This model, equipped with multi-head attention layers, allows the network to dynamically learn and weigh the interdependencies among various frequencies within the frequency spectrum. As a result, it demonstrates enhanced interpretability and broader applicability. Changming Li [7] proposed a deep learning (DL) method known as the Propeller Wake Convolutional Neural Network (PWCNN), which combines transformer encoders and dilated convolutional blocks to capture multi-scale features of the wake. Guo, X [8] has developed a novel method for automatically detecting photons reflected from the shallow seafloor using ICESat-2 altimetry data. Compared to the traditional multi-band ratio model, the backpropagation (BP) neural network model can effectively enhance the accuracy of depth sounding. This approach facilitates the easier acquisition of shallow water bathymetry without the need for in situ sounding data. Vicens-Miquel M [9] has put forth a resilient deep learning framework designed to forecast water levels across various tidal stations along the Gulf Coast, encompassing open shorelines, estuaries, and waterways adjacent to significant harbors. The chosen Seq2Seq architecture has demonstrated notable enhancements over prior research, aligning with the operational benchmarks set by the National Oceanic and Atmospheric Administration (NOAA). Specifically, the model achieves prediction accuracies within 15 cm for a forecast horizon of up to 108 h at the tide gauges in Port Isabel, with a success rate of 92.2%, and in Rockport, with a rate of 90.4%. Bolong Liu [10] proposed a method based on the optimization of backpropagation neural networks using a Genetic Algorithm (GA), specifically the Non-dominated Sorting Genetic Algorithm II (NSGA-II), to optimize the resistance performance under two different conditions. The optimized configuration parameters achieved a 22.71% energy saving ratio at cruising speed. Indu Kant Deo [11] proposed a deep learning technique for data-driven prediction of wave propagation in fluid media. Compared to the standard recurrent neural networks with long short-term memory units, the attention-based sequence-to-sequence networks increased the time range of predictions. Denoising autoencoders further reduced the mean squared error of predictions, enhancing the generalization capability across the parameter space. Jiao Y [12] addressed the issue of large errors in coastal sea surface temperature (SST) predictions from numerical models by employing the deep learning method LSTM to develop an optimal SST forecasting model. The LSTM-based SST prediction model effectively improved the accuracy of forecasts, reducing errors by an average of 78% compared to numerical models. Zhao X [13] investigated the application of convolutional neural networks (CNNs) and recurrent neural networks (RNNs) in hydrological forecasting, as well as their comparison. Zhuxin Ouyang [14] has introduced an integrated approach that marries empirical mode decomposition (EMD) with TimesNet, resulting

in the EMD-TimesNet model for significant wave height (SWH) prediction. This model is adept at forecasting SWH with precision across diverse marine environments. Xianrui Hou [15] has developed a short-term prediction technique for ship roll motion amidst waves, leveraging the power of convolutional neural networks (CNNs). This method has proven effective in accurately anticipating the ship's roll behavior in wave conditions. Yang Binghua [16] proposed a ship motion attitude ultra-short-term combined prediction model based on a self-attention mechanism and long short-term neural network to address the difficulty in accurately predicting ship motion attitudes. Fu Wanqian [17] developed an adaptive sequence parallel sampling method and a point-by-point ensemble model construction method to address the bottleneck challenges of long computation time and low efficiency faced by high-precision CFD modeling techniques for severely nonlinear motions of damaged ships in waves. Duan Shiliang [18] proposed a single-feature training deep learning model based on motion difference training, as well as two multi-feature training models: one using single-point significant wave height and wave steepness input, and the other using multi-point significant wave height input. Wang Kejun et al. [19] applied, fort the first time, the autoregressive neural network to the time-series forecasting of ship roll motion, achieving good predictive results. Xu Pei et al. [20] proposed a method that combines the backpropagation algorithm with the temporal differencing algorithm based on autoregressive neural networks, improving the forecasting capability of autoregressive neural networks.

This study is anchored in a rich dataset of marine environmental conditions and leverages the advanced learning capabilities of neural networks to identify and address complex nonlinear relationships within historical data, thereby enabling precise predictions of offshore platform motion responses. This contributes to the early detection of potential risks and accident prevention and provides robust technical support for the sustainable development of offshore energy and marine engineering. Initially, this study employs the STAR-CCM+2022.1 software for fluid dynamics simulation to obtain a dataset of offshore platform motion under various marine conditions. Subsequently, a combination of a residual convolutional neural network (ResCNN) and Long Short-Term Memory (LSTM) networks is utilized to forecast platform motion under different wave heights and wave direction angles. This research introduces the empirical mode decomposition (EMD) algorithm to enhance predictive accuracy, particularly under varying wave direction angles. Furthermore, the model's performance was strictly assessed with R^2, MSE, and MAPE, confirming the reliability and accuracy of the predictions.

2. Basic Theory

2.1. Principle of Neural Network

2.1.1. The Principle of the Long Short-Term Memory Neural Network

The Long Short-Term Memory (LSTM) neural network was crafted to tackle the challenges of vanishing or exploding gradients that traditional recurrent neural networks (RNNs) face when dealing with extended sequence data [21]. Such challenges restrict RNNs' capacity to maintain long-term dependencies. LSTM overcomes these limitations by incorporating gated units, which has led to its significant utility in domains like natural language processing, speech recognition, and time-series forecasting.

The core of the LSTM network lies in its unique cell state, which runs through the entire sequence, allowing information to be preserved or forgotten over long periods within the network [22]. The LSTM network consists of three key gated units: the forget gate, the input gate, and the output gate [23]. These gated units collectively determine the updating of the cell state and the final output of the hidden state.

The forget gate's function is to decide which information should be discarded from the cell state of the previous time step. This process is implemented through a fully connected layer with a sigmoid activation function, with output values ranging between 0 and 1, indicating the degree of information retention [24]. The input gate is responsible for determining which parts of the current time step's input information should be added

to the cell state to update it. The input gate consists of two parts: one part determines the acceptance weight of the information through a sigmoid function, and the other part calculates the candidate state through a tanh function, representing the potential value of new information [25]. The update of the cell state is a combination of the results of the forget gate and the input gate, carried out through element-wise multiplication. The output gate's function is to determine the value of the next hidden state, deciding which information in the cell state should be passed to the hidden state of the next moment or served as the model output at the current moment. The activation value of the output gate is also calculated through a fully connected layer with a sigmoid activation function, and then the final hidden state is obtained through element-wise multiplication with the cell state value after passing through the tanh function [26]. The computational formulas are as follows [27]:

$$f_t = \sigma(W_{xy}x_t + W_{hf}h_{t-1} + W_{cf}c_{t-1} + b_f) \tag{1}$$

$$i_t = \sigma(W_{xi}x_t + W_{hi}h_{t-1} + W_{ci}c_{t-1} + b_i) \tag{2}$$

$$c_t = f_t c_{t-1} + i_t \tanh(W_{xc}x_t + W_{hc}h_{t-1} + b_c) \tag{3}$$

$$o_t = \sigma(W_{xo}x_t + W_{ho}h_{t-1} + W_{co}c_t + b_o) \tag{4}$$

$$h_t = O_t \tanh(c_t) \tag{5}$$

In the provided equations, the first represents the calculation for the forget gate; the second denotes the input gate's activation at time step t; h_{t-1} signifies the output from the previous time step's hidden layer. The terms W and b correspond to the weight matrix and bias vector associated with the gate, respectively. The symbol σ represents the sigmoid activation function. The third equation pertains to the input gate, which is responsible for updating the cell state. Lastly, the fourth equation describes the output gate, which, in conjunction with the cell state, generates the output h_t.

2.1.2. Convolution Layer Principle

One-dimensional convolutional layers are pivotal components within convolutional neural networks, specifically tailored for processing one-dimensional data. These layers employ local connectivity, weight sharing, and sparse connectivity to slide a kernel across the input sequence, applying the same convolutional filter to extract local features [28]. This architecture not only diminishes the number of model parameters and computational complexity but also bolsters the model's invariance to translations in the input data. The utilization of multiple convolutional kernels enables the network to capture a diverse array of features, while the incorporation of activation functions introduces nonlinear capabilities to the model [29]. This structure is particularly adept at handling one-dimensional sequences such as time-series data and audio signals, rendering it highly effective in tasks such as speech recognition and time-series prediction.

In the context of research, the convolutional layer used is a one-dimensional variant optimized for sequence data processing. Figure 1 illustrates one-dimensional convolution with a kernel sliding over the input sequence, multiplying and summing to produce output elements [30]. This process is repeated as the kernel moves across the entire sequence, culminating in the formation of a new sequence that encapsulates the convolutional output between the kernel and the original sequence. This approach effectively captures the temporal dependencies within the data, providing a robust framework for analyzing sequential information [31].
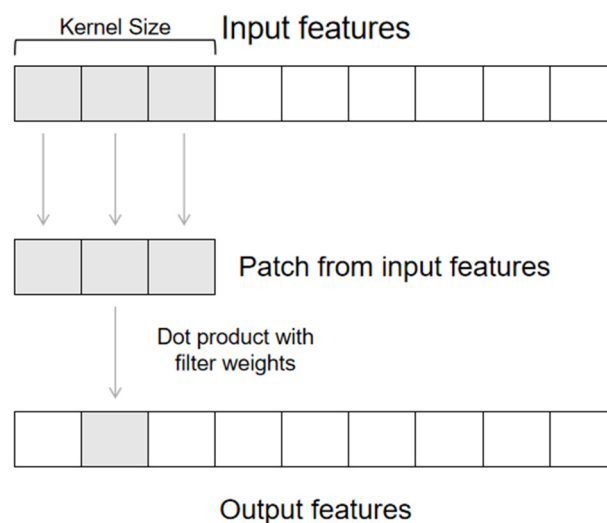
Figure 1. Diagram of one-dimensional convolution operation [32].

2.2. Performance Evaluation Index

After training a machine learning model, evaluating its predictive accuracy and making improvements based on the results is essential. This study uses three primary metrics to assess the model's predictive performance: the coefficient of determination (R^2), mean squared error (MSE), and Mean Absolute Percentage Error (MAPE) [33].

The coefficient of determination (R^2) measures the proportion of the variance in the actual data that is predictable from the model's predictions. It reflects the model's fit to the data, with values approaching 1 indicating a better fit. Unlike other squared metrics, R^2 can be negative, suggesting a poor fit when values are low [34]. In the realm of offshore platform motion response prediction, a high R^2 value signifies the model's ability to capture the intricate dynamics of platform motion, which is crucial for the accuracy and reliability of the forecasts.

The mean squared error (MSE) and Mean Absolute Percentage Error (MAPE) both measure the differences between the model's predictions and actual values. MSE calculates the average of the squared differences across all samples, providing a measure of the prediction errors' magnitude. Conversely, MAPE calculates the average of the absolute relative errors for all samples, offering a percentage-based error measure. Both MSE and MAPE are non-negative, with lower values indicating better model performance, as they suggest smaller prediction errors [35]. In offshore platform motion response prediction, MSE offers a quantitative measure of error, aiding engineers in evaluating and refining models to reduce predictive errors and enhance platform stability and safety. MAPE provides insight into the relative magnitude of prediction errors, which is essential for assessing the model's applicability and robustness under various sea conditions. A low MAPE value indicates that the model's predictions closely match actual observations, which is vital for operational decision-making and risk management on offshore platforms.

3. Prediction Analysis of Motion Response of Offshore Platform Under Multiple Sea State Condition Samples

*3.1. Establishment of Neural Network Model*

Long Short-Term Memory (LSTM) networks demonstrate superior performance compared to Gated Recurrent Units (GRUs), Bidirectional Long Short-Term Memory (BiLSTM), and Bidirectional Gated Recurrent Units (BiGRUs) due to their sophisticated gating mechanisms that adeptly manage long-term dependencies. The LSTM's memory cell enables selective information retention across time sequences, which is essential for complex sequential tasks. While GRUs offer a simplified structure with faster training times, LSTM networks' detailed control mechanisms typically yield better performance in tasks involving intricate long-term dependencies. Although BiLSTM and BiGRUs provide comprehensive

sequence understanding through bidirectional processing, LSTM's unidirectional approach offers greater computational efficiency through reduced parameter count. However, LSTM exhibits limitations in feature extraction from highly nonlinear data.

To address the limitations of LSTM in handling nonlinear data, this study incorporates convolutional layers to fully leverage the spatial features within the dataset. These layers capture local patterns and contribute to a comprehensive feature representation, enhancing the model's ability to understand data complexity and improve prediction accuracy. By increasing the number of convolutional layers, the model deepens, thereby strengthening its feature extraction capabilities. Furthermore, a residual structure utilizing skip connections is implemented to combine multi-level feature extraction results effectively. In one-dimensional signal processing, ResCNNs outperform alternative methods such as Independent Component Analysis (ICA), Fast ICA (FICA), Recursive Least Squares (RLSs) filters, wavelet transforms (WTs), and Deep Neural Networks (DNNs) due to its deep architecture, which automatically extracts complex nonlinear features from signals. The end-to-end processing capability simplifies workflow by directly mapping noisy signals to clean ones, eliminating extensive preprocessing requirements. ResCNNs' multi-scale feature fusion enables comprehensive capture of both local and global signal characteristics, enhancing perceptual ability and facilitating precise extraction of motion characteristics and dynamic change analysis.

The convolution sub-module comprises convolutional layers, standardization layers, and hidden layers, while the loop operation module includes two LSTM layers, two hidden layers, and two dropout layers. By integrating the strengths of these two algorithms, compared to traditional forecasting models such as RNNs, LSTM, and GRUs, the capability to learn deep features on the temporal dimension has been significantly enhanced, as has the accuracy of predicting time-series trends on the temporal dimension. The model effectively captures intrinsic characteristics data, overcoming the limitations of traditional forecasting algorithms when dealing with complex and highly nonlinear datasets. Furthermore, the synergistic interaction between spatial and temporal dimensions enables the model to more effectively learn key features within the data, demonstrating significant advantages in data analysis and prediction applications. The calculation process is shown in Figure 2.
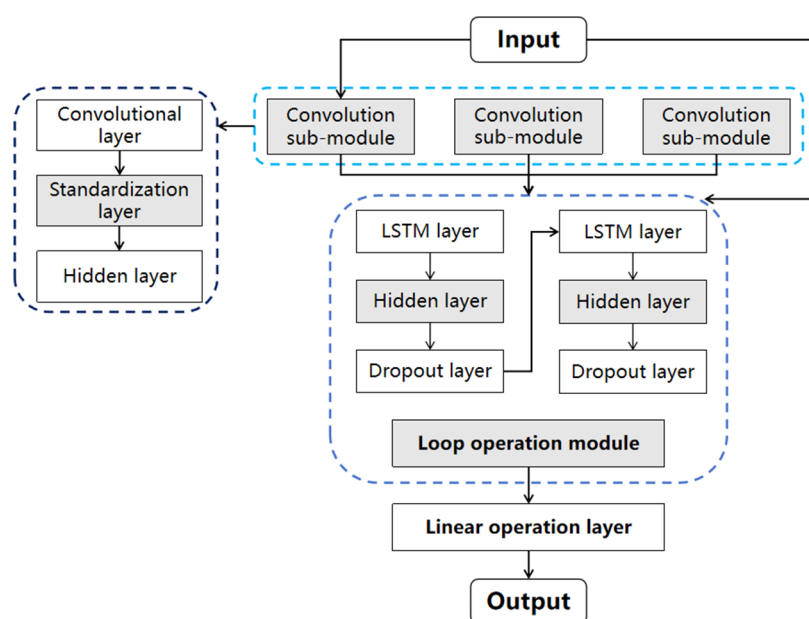
**Figure 2.** Computational flow graph of ResCNN−LSTM.

The predictive model in this study was developed using Python 3.8.5, utilizing the following key libraries with their respective versions: NumPy 1.18.0 for numerical operations,

Pandas 1.1.3 for data manipulation, Matplotlib 3.3.2 for plotting, and TensorFlow 2.2.3 for deep learning model development.

Subsequently, this model will be referred to as ResCNN-LSTM.

3.2. Platform Model Establishment

This research focuses on a semi-submersible offshore platform, characterized by its structural composition that encompasses an upper deck, four columns with chamfered edges, a pair of cylindrical cross braces, and a duo of buoyancy tanks, as depicted in Figure 3. The geometric parameters of this platform are meticulously detailed in Table 1 [36].
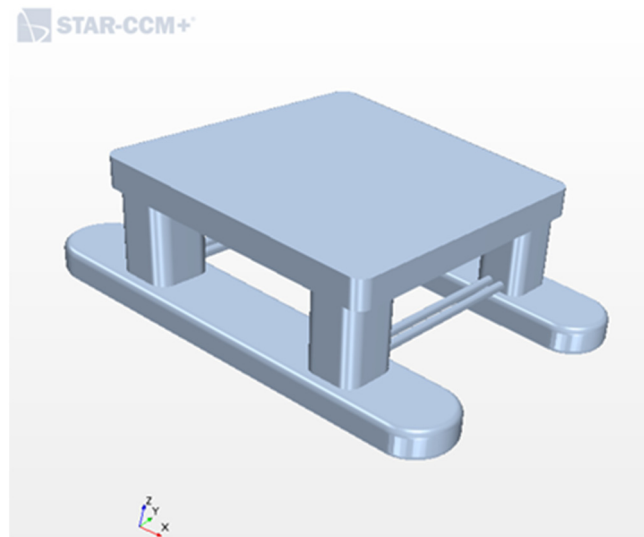
Figure 3. Model diagram of the semi-submersible offshore platform.

Table 1. Geometric parameters of the semi-submersible offshore platform.

Parameter	Magnitude	Unit
Molded length	58.0	m
Molded breadth	40.0	m
Deck length	39.4	m
Deck width	37.8	m
Main body height	19.2	m
Column height	10.9	m
Column section	7.2×7.2	m
Transverse brace diameter	1.25	m

During the numerical simulation of the original platform model, due to the significant computational resources demanded by the viscous flow field calculations, a scaled-down model with a reduction ratio of 1:50 was employed for the computational analysis. Table 2 presents a comparative analysis of the operational parameters between the original and scaled models. This scaling approach was implemented to optimize computational resource utilization.

Table 2. The working condition parameters of the original model and the scale model of the platform.

Parameter	Platform Original Model	Scale Model
Drainage volume	5.53×10^6 kg	44.21 kg
Draught	6.897 m	0.1379 m
Height of center of gravity	6.615 m	0.1323 m
Roll moment of inertia	1.08×10^9 kg·m^2	3.46 kg·m^2
Pitching moment of inertia	1.19×10^9 kg·m^2	3.81 kg·m^2
Bow moment of inertia	1.56 kg·m^2	5.01 kg·m^2

3.3. Adaptive Analysis of Wave Direction Angle

The numerical wave tank was configured according to the dimensions of the scaled-down model, with specific dimensions of 15 m in length, 8 m in width, and 5.5 m in molding depth. The model was established based on the origin, and after scaling down, the draft is 0.1379 m. Consequently, the water surface height was adjusted upward by 0.1379 m, resulting in a wave flume depth of 4.1379 m below the waterline. The computational domain for numerical simulations comprises a quiescent zone and an overlapping zone, wherein the quiescent zone is designated as the wave propagation region. The direction of the *X*-axis is defined as the wave incidence direction, with the angle of wave incidence set at $0°$. The parameters of the wave are detailed in Table 3.

Table 3. Parameters of wave.

	Significant Wave Height	Spectrum Peak Period	Number of Wave Components	Incidence Angle
Condition one	0.1	1.56 s	75	0°
Condition two	0.1	1.56 s	75	45°

The framework uses a turbulence model and an implicit, unsteady time solver with second-order time discretization. To reduce wave reflection at the outlet boundary, an 8 m-long damping zone is implemented, utilizing the Volume of Fluid (VOF) method for wave simulation.

Figure 4 depicts the numerical computation domain.

To ensure simulation accuracy, an overlapping grid method was employed for the simulation of the ship's motion. The ship and a portion of the surrounding fluid domain were meshed separately, with the ship and its immediate area designated as the overlapping region. Under the condition of releasing certain degrees of freedom (heave and pitch), the overlapping region was allowed to move within the scope of the background domain. Data exchange between the overlapping and background grids was facilitated through interpolation, thereby obtaining flow field information across the entire fluid domain.

The meshing process employed in this study uses the STAR-CCM+ software, which incorporates surface reconstruction, a cutting body mesh generator, and a prism layer mesh generator for mesh division. This approach, combined with overlapping mesh technology, efficiently generates high-quality meshes. Within the numerical pool, the cutting body mesh generator is used to produce high-quality hexahedral meshes. The prism layer mesh consists of six layers with an extension rate of 1.2, resulting in a total mesh count of 2.61 million. The specific grid division is illustrated in Figure 5.

After conducting numerical simulation for the aforementioned conditions, the motion time histories are depicted in Figures 6 and 7. The numerical simulation lasts for 500 s with a time step of 0.01 s, yielding 50,000 time steps for both heave and pitch data. Only a portion of the time histories is displayed in the figures.

The dataset was divided into training and testing subsets in a 7:3 ratio, following the chronological order of the data. This study employs an advanced forecasting strategy known as multi-step prediction, which analyzes motion data over twice the time duration to predict the subsequent half-time duration of motion. Given that the marine platform model used is scaled down according to a specific ratio, its motion period is also reduced in accordance with Froude's number principle to ensure dynamic similarity between model tests and real-world conditions. The focus of this paper is to demonstrate the effectiveness of this predictive method. Therefore, under the condition of reduced motion periods, we selected motion posture data spanning four seconds as the input to predict the following two seconds of motion posture, thereby validating our methodology.
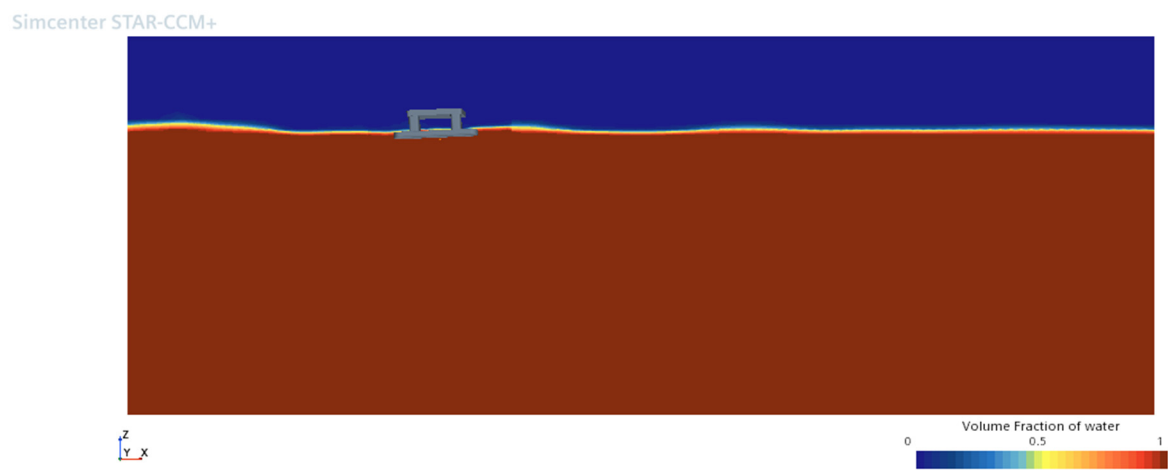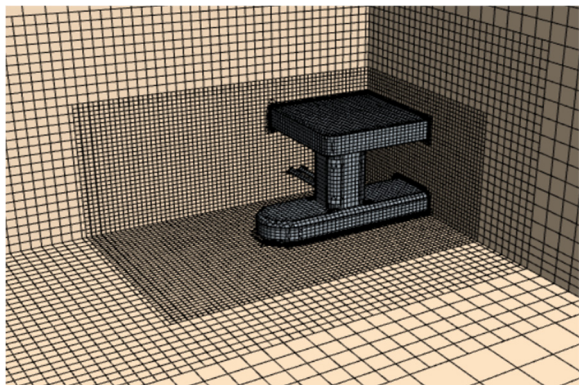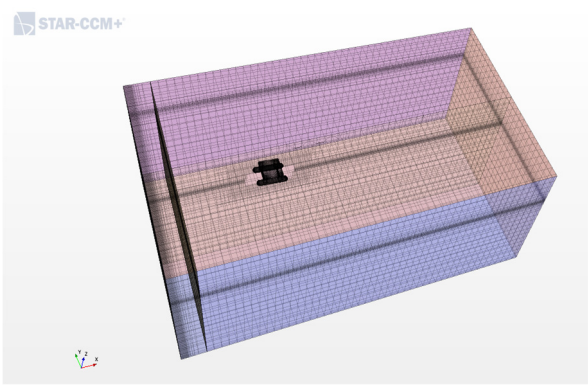
(**a**)
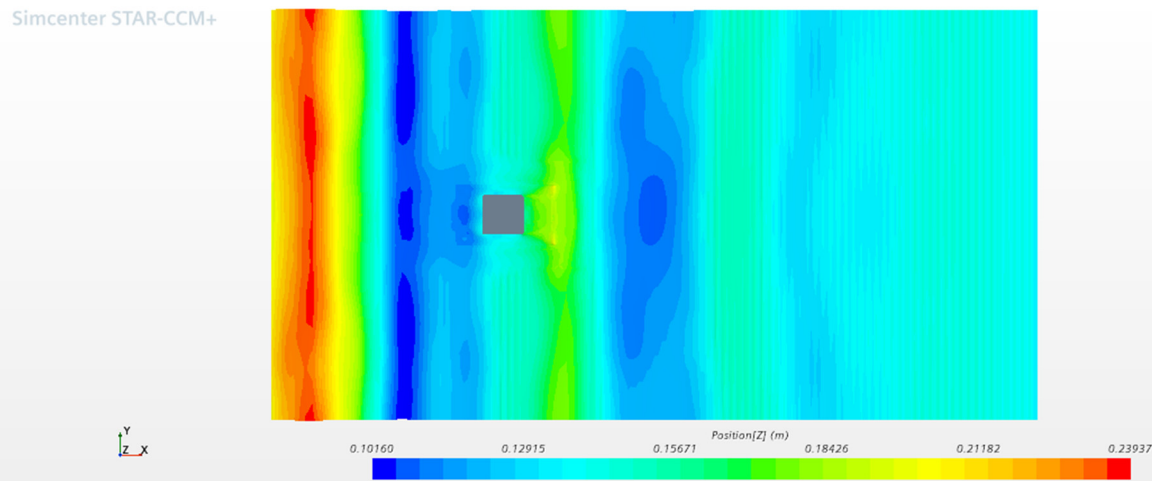
(**b**)

Figure 4. Numerical computation field. (**a**) Distribution diagram of water and gas phases; (**b**) flow field propagation.
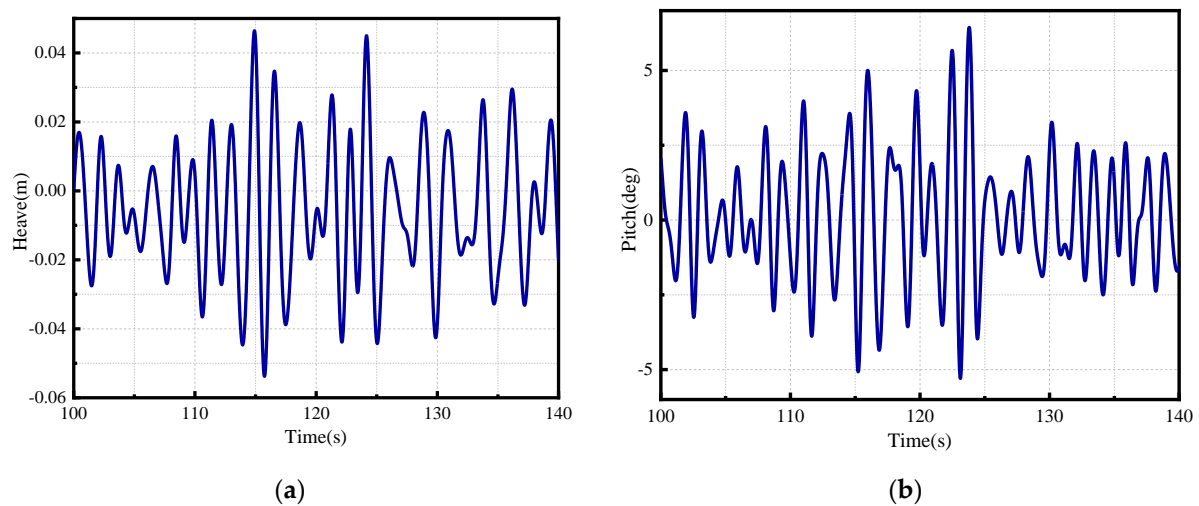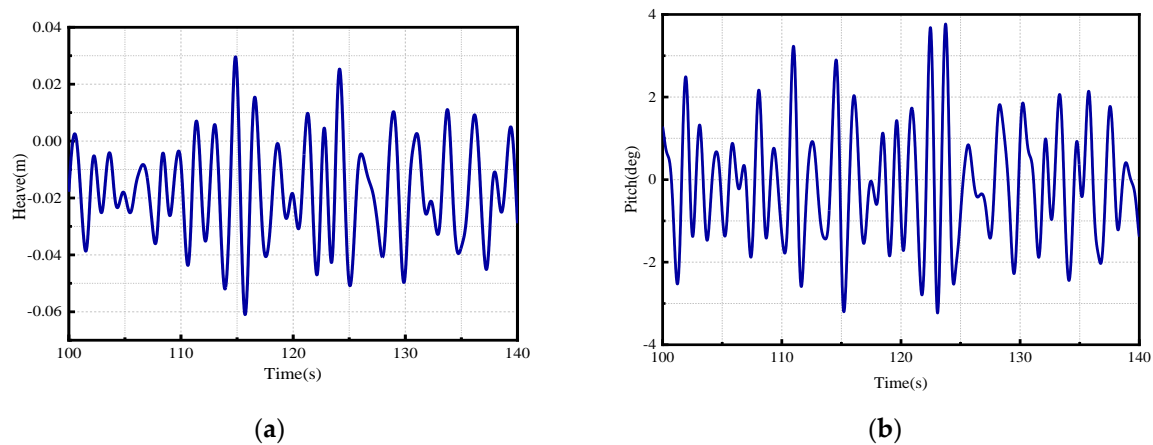

(**a**)   (**b**)

Figure 5. Grid division situation. (**a**) Model encryption. (**b**) Flow field encryption.

(a)

(b)

Figure 6. Time history curve of local motion in working condition one. (**a**) Local diagram of 100−140 s heave motion. (**b**) Local diagram of 100−140 s pitch motion.

(a)

(b)

Figure 7. Time history curve of local motion in working condition two. (**a**) Local diagram of 100−140 s heave motion. (**b**) Local diagram of 100−140 s pitch motion.

The number and size of convolutional kernels influence the model's receptive field, feature extraction capabilities, and computational complexity. Activation functions introduce nonlinearity into neural networks, control neuron activation, and affect learning speed, convergence, and model generalization. The choice of the hyperbolic tangent function is attributed to its centered output, smoothness, and favorable gradient properties, which contribute to enhancing the training efficiency and generalization capability of neural networks. Optimizers adjust parameters during model training to minimize loss functions and improve model performance. The selection of the Adam optimizer is based on its ability to adaptively adjust the learning rate for individual parameters, combining the advantages of both momentum and RMSProp. Additionally, it exhibits robustness in hyperparameter sensitivity, typically delivering satisfactory performance across a range of tasks with minimal tuning required. The initial training learning rate determines the step size of model parameter updates at the beginning of training, influencing the learning speed and convergence. During hyperparameter tuning, the following kernel sizes were tested for the two LSTM layers: 128 and 64, 256 and 128, and 512 and 256. After comparing the error situations, the combination of 256 and 128 was deemed most suitable. The number and size of kernels in the convolutional layer are 2 and 4. The learning rate is 0.001, with 100 training epochs.

It is worth noting that after splitting the training set into individual samples, they are shuffled randomly before being input into the model for training. This helps reduce the

model's attention to background noise, decrease sensitivity to missing data, and improve the robustness of the model. Additionally, the order of the testing set data is kept unchanged to ensure that the model's predictions reflect the time-series information for analysis. The prediction results are shown in Figure 8, where, due to the large number of samples, one single sample for heave and pitch motion from each of the two conditions is selected for demonstration of the results.

(a)

(b)

(c)

(d)
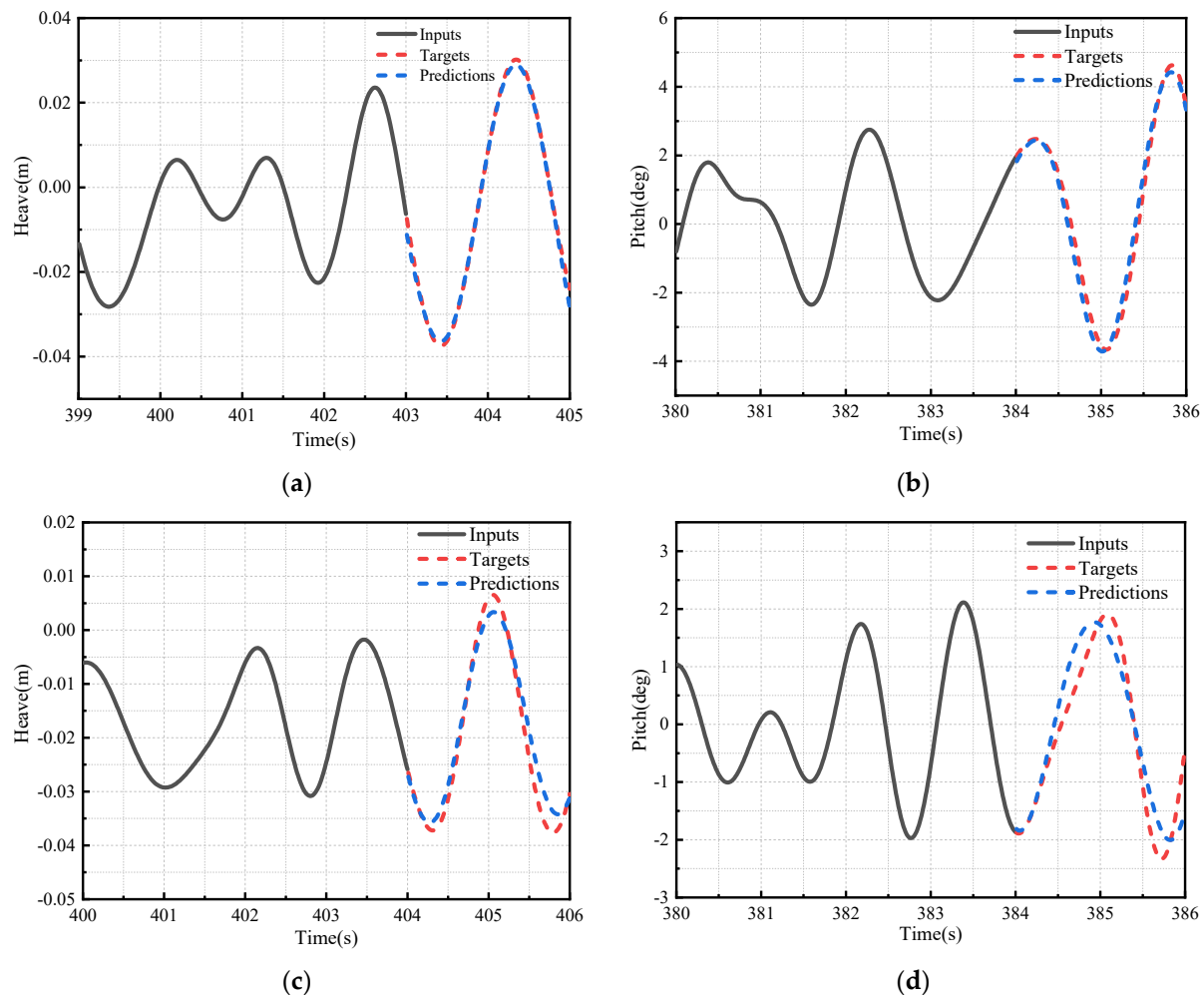
Figure 8. Diagram of individual predictions on the test set. (**a**) Single sample of 0−degree incident angle heave test set, (**b**) 0−degree incident angle pitch test set single sample, (**c**) 45−degree incident angle heave test set single sample, and (**d**) 45−degree incident angle pitch test set single sample.

The model's ability to capture trends and variations in individual sample motion is evident when observing the predicted time history curves. These curves demonstrate the model's accurate predictions. To objectively assess the model's predictive capabilities, the R^2 metric is used for evaluation. This metric provides a more objective assessment of the model's predictive capabilities and understanding of its accuracy at different time steps, as shown in Figure 9.
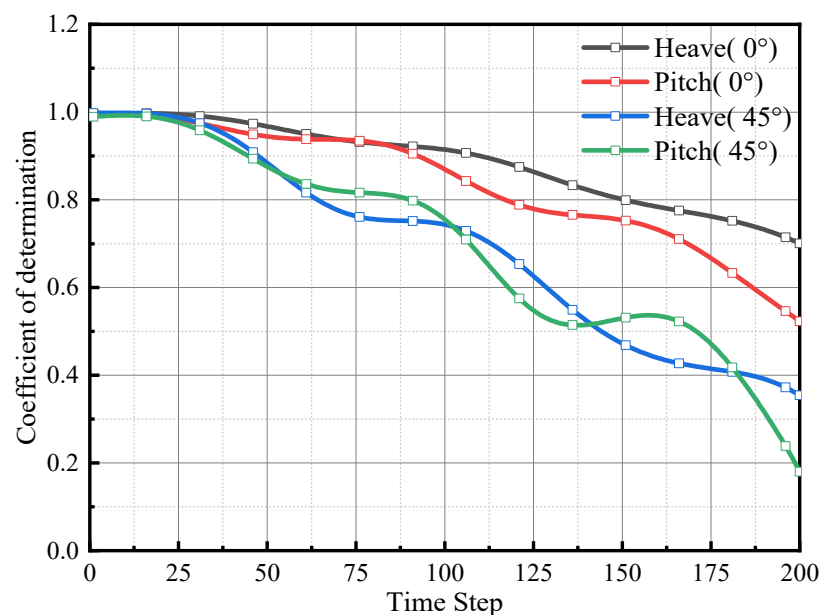
Figure 9. R^2 comparison diagram.

The figure reveals that for wave incident angles of 0 and 45 degrees, the model successfully predicts heave and pitch motions of the offshore platform throughout the entire time period. An R^2 value of 1 signifies a perfect match between predicted and true values, with values closer to 1 indicating better performance. Examining the heave and pitch motions for a wave incident angle of 0 degrees, it is evident that the R^2 values for both motions remain consistently above 0.5 across the entire predicted time steps. This highlights the model's robust predictive capability for these motions. While a slight downward trend in prediction accuracy is observed over time, this is typical in multi-step forecasting due to increasing uncertainty and data variability. The gradual nature of this decline indicates a balanced and stable overall prediction performance, emphasizing the model's consistency and accuracy throughout the process.

Regarding the 45-degree wave incident angle, the overall R^2 values show a slight decrease compared to the 0-degree scenario. This reduction can be attributed to the increased impact experienced by the offshore platform at this angle, leading to more pronounced nonlinear motions and greater irregularity in motion patterns. The pitch motion, in particular, is significantly affected by fluid resonance issues, making prediction more challenging. Despite these challenges, the R^2 values for heave motion remain above 0.3 throughout the entire predicted time span, while those for pitch motion generally exceed 0.2. This indicates that the model maintains its predictive capability without any instances of failed fitting.

3.4. Adaptive Analysis of Significant Wave Height

An adaptive study on the significant wave height has been conducted to predict the heave and pitch motions of offshore platforms with the same wave direction angle but varying significant wave heights. The numerical wave tank and mesh refinement settings are identical to those in Section 3.3 Specific wave parameters are detailed in Table 4.

Table 4. Operating parameters.

	Significant Wave Height	Spectrum Peak Period	Number of Wave Components	Incidence Angle
Condition one	0.07	1.41 s	75	0°
Condition two	0.1	1.56 s	75	0°

After conducting numerical simulation for the aforementioned conditions, the motion time histories are depicted in Figures 10 and 11. Because of the numerical simulation spanning 500 s, only partial time histories are displayed.


(**a**)   (**b**)
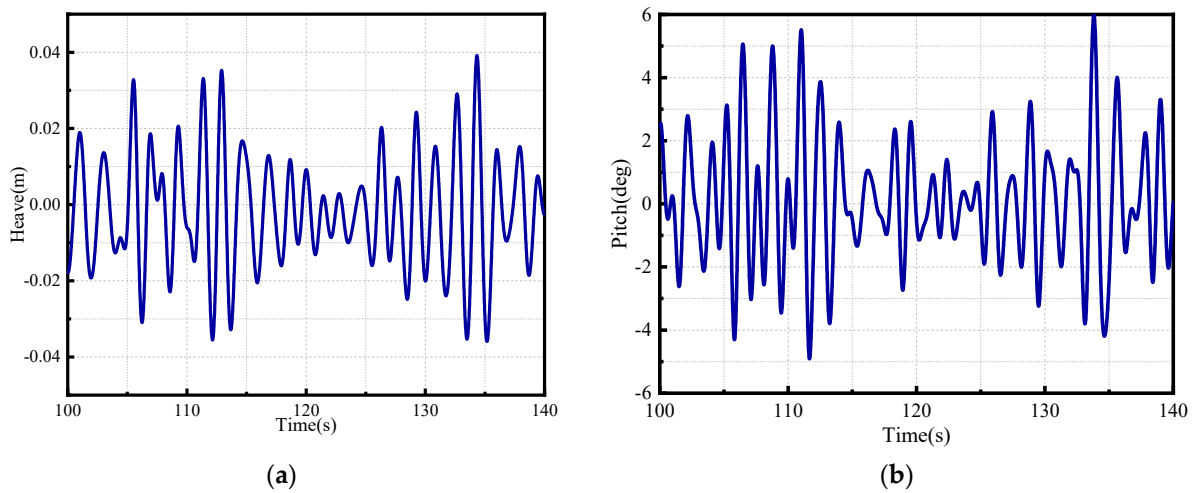
Figure 10. Time history curve of local motion in working condition one. (**a**) Local diagram of 100−140 s heave motion. (**b**) Local diagram of 100−140 s pitch motion.

(**a**)   (**b**)
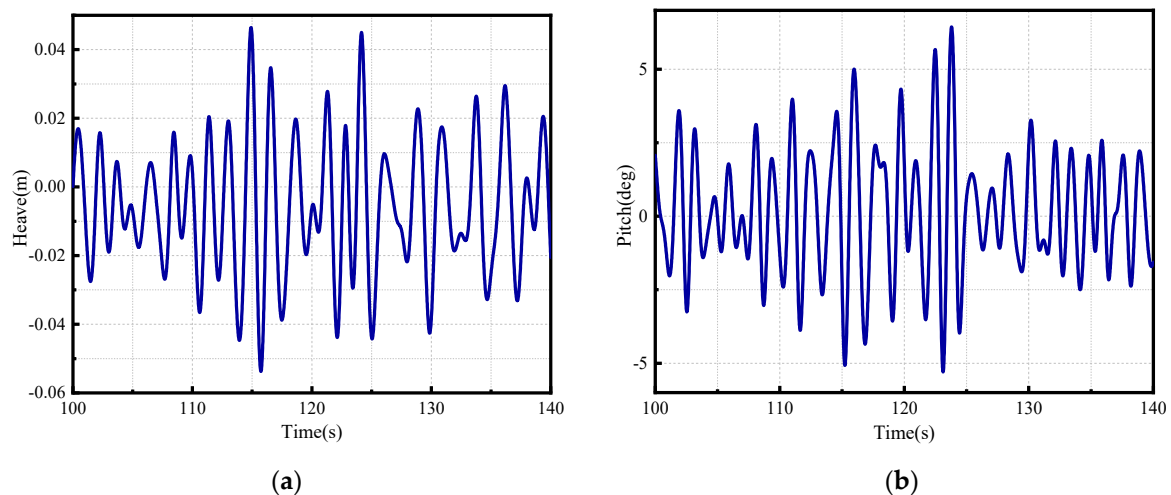
Figure 11. Time history curve of local motion in working condition two. (**a**) Local diagram of 100−140 s heave motion. (**b**) Local diagram of 100−140 s pitch motion.

The sample set division strategy and prediction strategy are consistent with the previous section. After shuffling the training set, it is inputted into the model for training. The parameters of the forecasting model are basically the same as those in Section 3.3. The prediction results are shown in Figure 12, where, due to the large number of samples, one single sample for heave and pitch motion from each of the two conditions is selected for demonstration of the results.
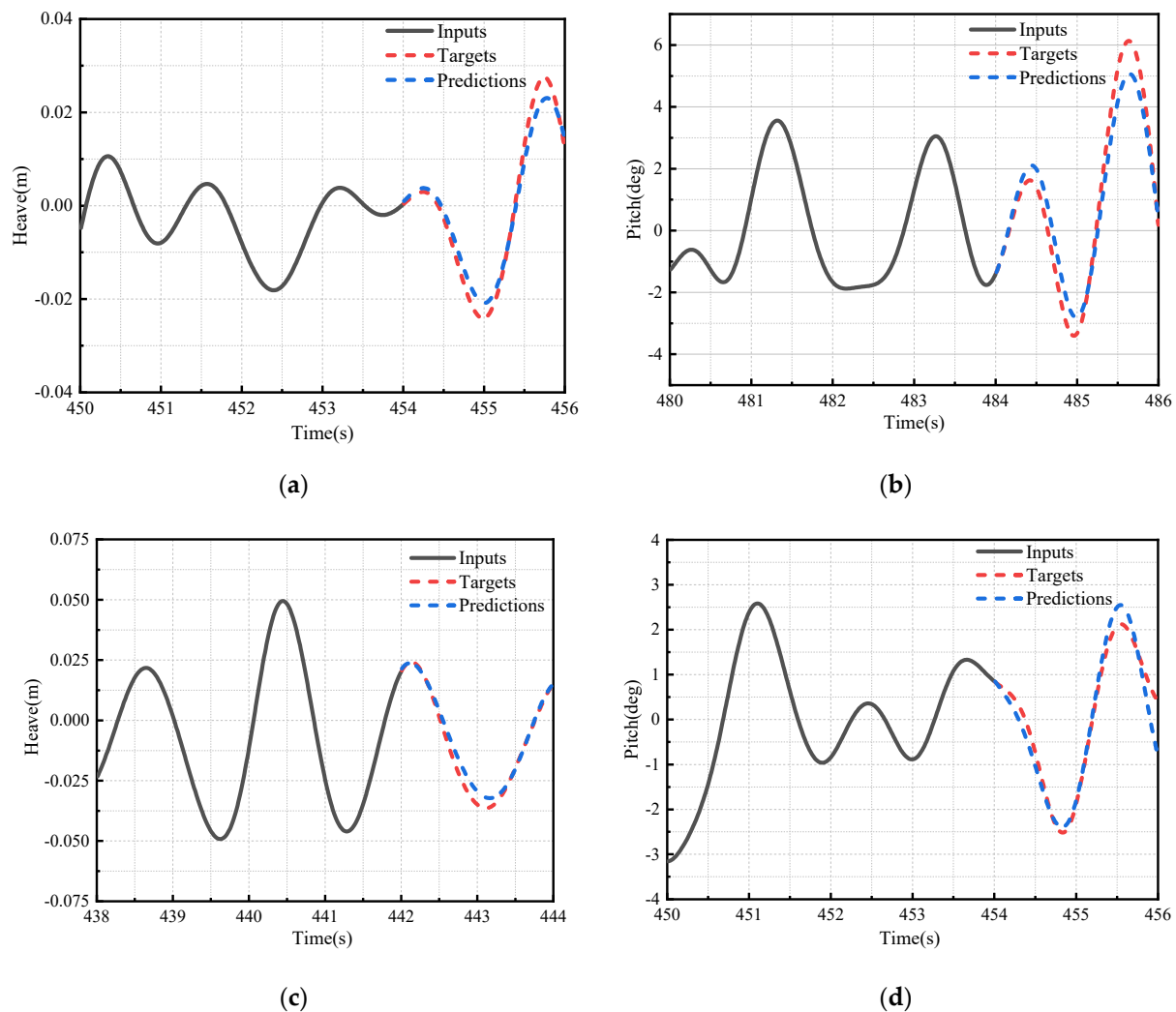
Figure 12. Diagram of individual predictions on the test set. (**a**) Heave test set single sample (H1/3 = 0.07 m). (**b**) Pitch test set single sample (H1/3 = 0.07 m). (**c**) Heave test set single sample (H1/3 = 0.1 m). (**d**) Pitch test set single sample (H1/3 = 0.1 m).

Figure 12 clearly demonstrates the model's excellent performance in predicting the heave and pitch motions of the offshore platform under varying significant wave heights. The time history curves show well-aligned rising and falling trends, indicating the model's ability to accurately capture the platform's motion patterns. To further evaluate the prediction performance, the R^2 metric is utilized, as illustrated in Figure 13.

Analysis of the heave motion reveals that the R^2 values exhibit minimal disparity between the two operational scenarios, maintaining consistent predictive accuracy throughout the entire forecasting horizon. This suggests that the model maintains stable predictive capabilities for heave motion even under varying significant wave heights, indicating a degree of adaptability. Similarly, examination of the pitch motion shows that the R^2 values display marginal variance over the predicted time steps, reflecting consistent predictive performance. Although the prediction accuracy for pitch motion slightly lags behind that of heave motion, the overall R^2 values generally exceed 0.4, with no instances of fitting failure.
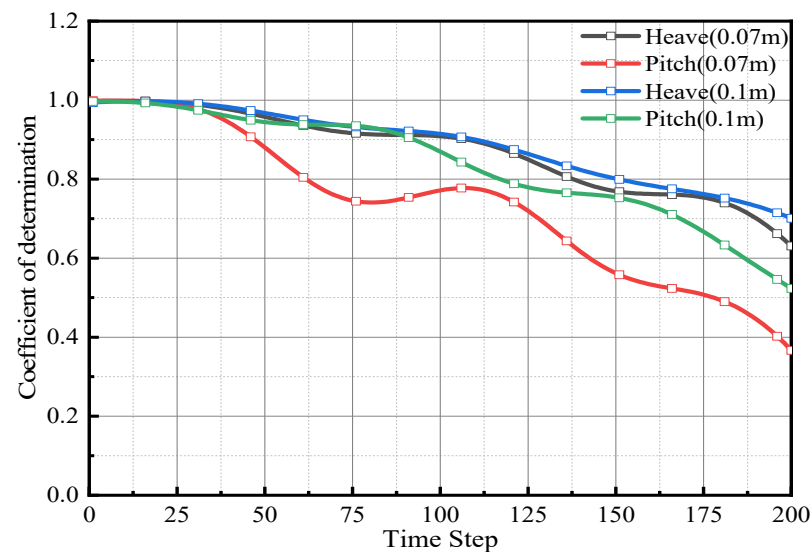
Figure 13. R^2 comparison diagram.

In summary, the effects of different significant wave heights on the prediction model for heave and pitch motions are relatively negligible, showing comparable performance across the two operating conditions and demonstrating a relatively balanced performance. This indicates that the model has good adaptability to the motion time history curves under different significant wave height conditions. However, the influence of different wave directions on the heave and pitch motions has a relatively significant impact on the prediction model. The predictions vary greatly between the two scenarios due to the different motion frequencies present under different wave directions. These frequency differences are challenging to eliminate through neural networks, thus causing the model to struggle to adapt well to these intricate motion patterns, presenting a challenging aspect for prediction. To address this issue, further optimization of the prediction model is necessary to better capture the frequency differences in motion under different wave directions and enhance the accuracy of the prediction model.

4. Improved Motion Response Prediction Model Based on EMD Algorithm

4.1. Construct EMD-ResCNN-LSTM Model

The empirical mode decomposition (EMD) algorithm is a signal processing technique specifically designed for analyzing nonlinear and non-stationary signals [37]. In time-signal processing, various alternative methods exist for signal decomposition besides empirical mode decomposition (EMD), including Ensemble Empirical Mode Decomposition (EEMD), Complementary Ensemble Empirical Mode Decomposition (CEEMD), Complete Ensemble Empirical Mode Decomposition with Adaptive Noise (CEEMDAN), Extreme Point Symmetric Mode Decomposition (ESMD), Variational Mode Decomposition (VMD), and Local Mean Decomposition (LMD) [38]. Despite these alternatives' advantages, EMD is often preferred for its adaptability and direct applicability to the analysis of non-stationary signals. This method differs from traditional time-series analysis techniques such as Fourier analysis or wavelet transforms in that it decomposes the signal based on their intrinsic properties without requiring specific basis functions. It automatically separates the original signal into multiple Intrinsic Mode Functions (IMFs) and a trend component (Residue), thereby avoiding the subjectivity associated with manually selecting basis functions and demonstrating its adaptive characteristics [39].

Integrating the empirical mode decomposition (EMD) algorithm with the ResCNN-LSTM forecasting method can significantly enhance the accuracy and applicability of time-series prediction models [40]. Compared to traditional forecasting models and the aforementioned ResCNN-LSTM, this combination provides a more comprehensive understanding of signal characteristics. It effectively analyzes signal frequency changes,

accurately extracts the Intrinsic Mode Functions (IMFs) and trend components, and precisely captures the instantaneous frequency of the signal, providing valuable input for subsequent predictions. This approach is particularly suitable for forecasting the heave and pitch motions under different wave incidence angles. The integration substantially improves the model's accuracy and applicability, aligning well with the data's actual physical significance. Compared to traditional CFD (Computational Fluid Dynamics) numerical predictions, the computational resources required for this model's predictions are significantly reduced, resulting in lower computational costs.

Hence, this section presents a predictive approach utilizing the combined EMD-ResCNN-LSTM model, specifically aimed at conducting ultra-short-term forecasts for offshore platform motion responses under diverse wave incident angles. Figure 14 vividly depicts the EMD decomposition process, providing a clear illustration of the signal decomposition procedure. Similarly, Figure 15 delineates the prediction methodology of the EMD-ResCNN-LSTM model, offering readers a detailed and intuitive reference for understanding and implementing the model.
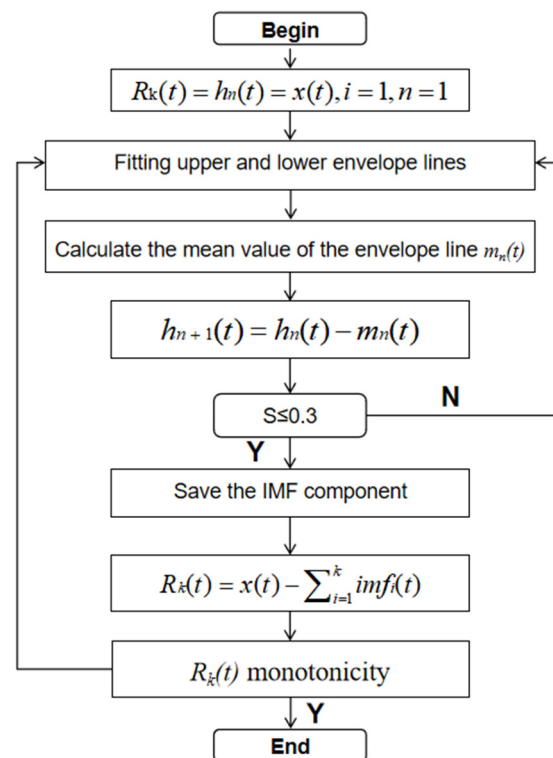

Begin

$R_k(t) = h_m(t) = x(t), i = 1, n = 1$

Fitting upper and lower envelope lines

Calculate the mean value of the envelope line $m_n(t)$

$h_{n+1}(t) = h_n(t) - m_n(t)$

$S \leq 0.3$ **N**

Y

Save the IMF component

$R_k(t) = x(t) - \sum_{i=1}^{k} imf_i(t)$

$R_k(t)$ monotonicity **Y**

End
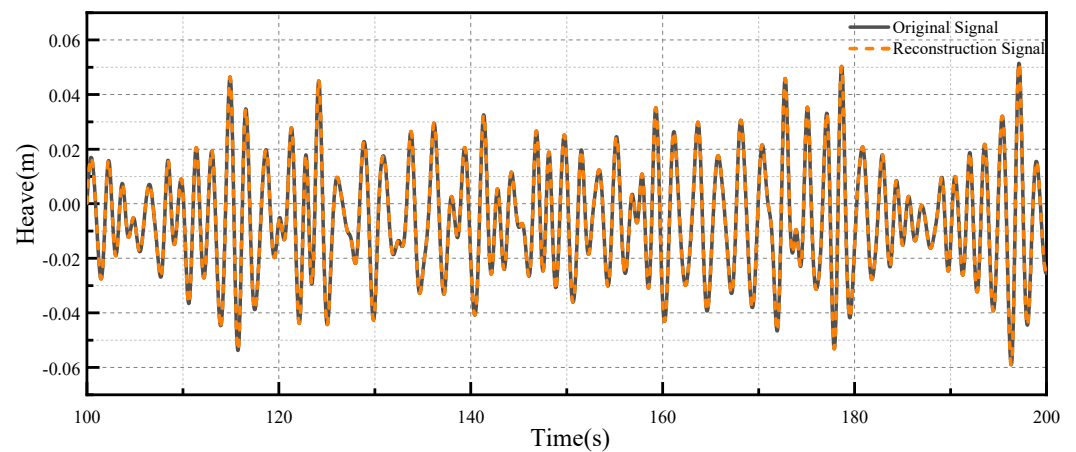
Figure 14. EMD algorithm decomposition flow chart.

4.2. Prediction Results and Error Analysis

This section employs the offshore platform motion response data under different wave incident angles provided in Section 2.2 as the dataset for analyzing and predicting model performance. To evaluate the empirical mode decomposition algorithm's decomposition capability, heave data from operational condition one were selected as the test sample. The EMD algorithm was applied to decompose the sample data, yielding a series of intrinsic mode function components and a trend component. These components and the trend component were then combined to reconstruct the original signal.

Comparison between the reconstructed and the original signal revealed high similarity, as shown in Figure 16, with the reconstruction error effectively controlled below 10^{-8} m. This finding strongly demonstrates the EMD algorithm's efficiency in handling non-stationary signals. It not only accurately decomposes the signal but also reliably reconstructs the original signal, which is crucial for practical engineering applications.

(**a**)

(**b**)
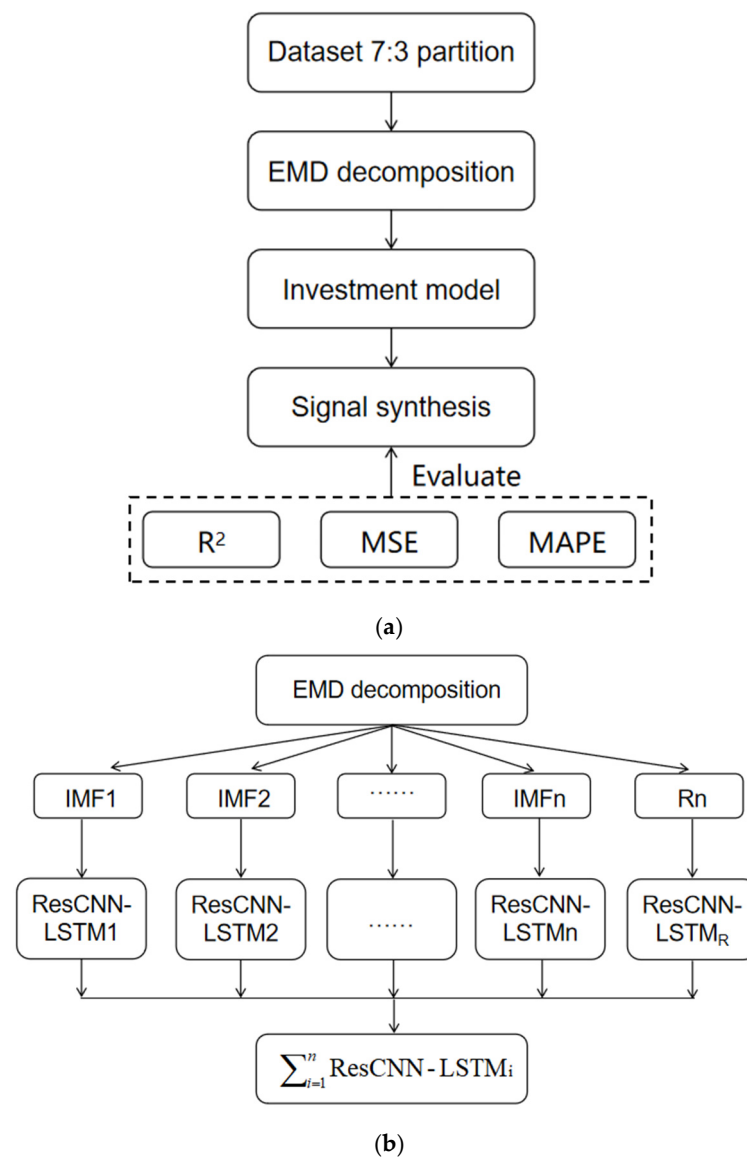
Figure 15. Prediction process and model structure. (**a**) Prediction process; (**b**) EMD-ResCNN-LSTM model flow chart.

Figure 16. Original signal and reconstructed signal.

After validating the EMD algorithm's effectiveness through verification, it was applied to decompose and process the data. Detailed decomposition analysis was conducted on the heave and pitch data recorded under different operational conditions. Due to the substantial volume of post-decomposition data, Figure 17 presents only the decomposition results of the heave motion data under operational condition one.

The IMF components and residuals obtained from the EMD decomposition of heave and pitch motion data under operational conditions one and two were used to establish ResCNN-LSTM models. The data were split into training and testing sets in a 7:3 ratio. A multi-step prediction approach was implemented, using four seconds of motion data as the input to predict the subsequent two seconds. Consequently, the input layer comprises 400 nodes, while the output layer contains 200 nodes. The mean squared error of the multidimensional output served as the loss function, with Adam as the optimization algorithm. Training continued for 100 epochs with an initial learning rate of 0.001. To facilitate comparison, the predictive outcomes of the EMD-ResCNN-LSTM model under two operational conditions are compared with the ResCNN-LSTM model. Due to the large sample size, two individual samples from each operational condition's heave and pitch test sets were randomly selected for demonstration, as illustrated in Figures 18–21.
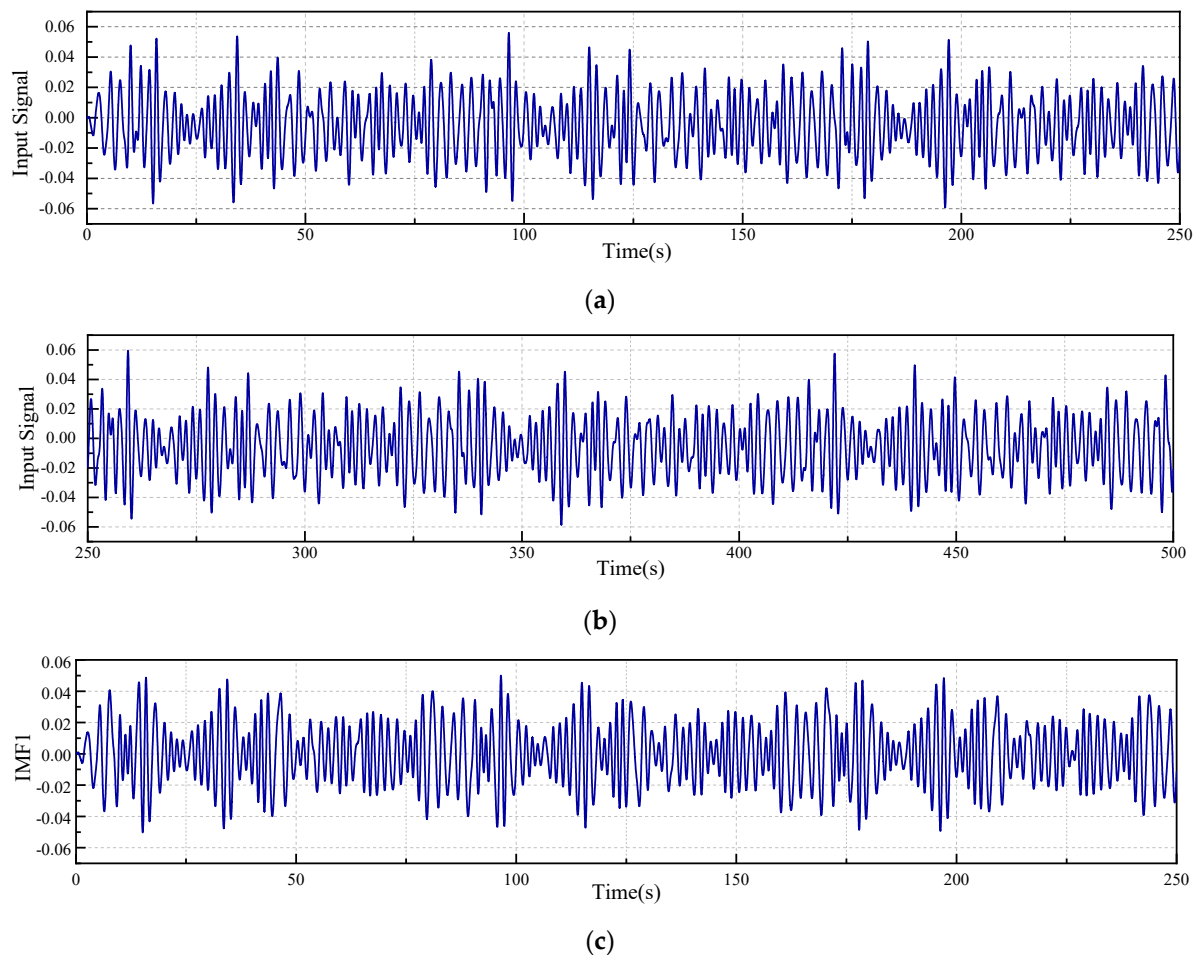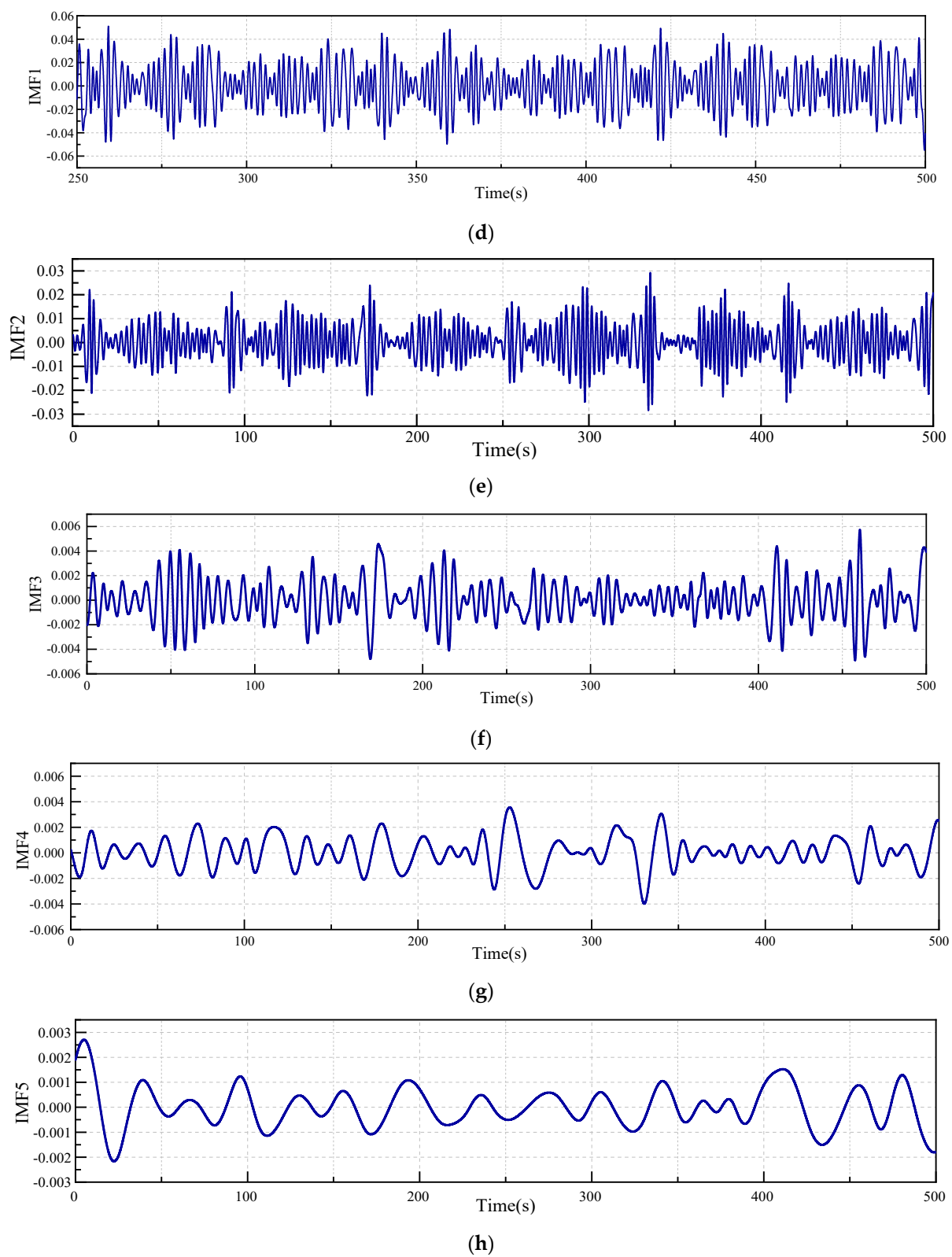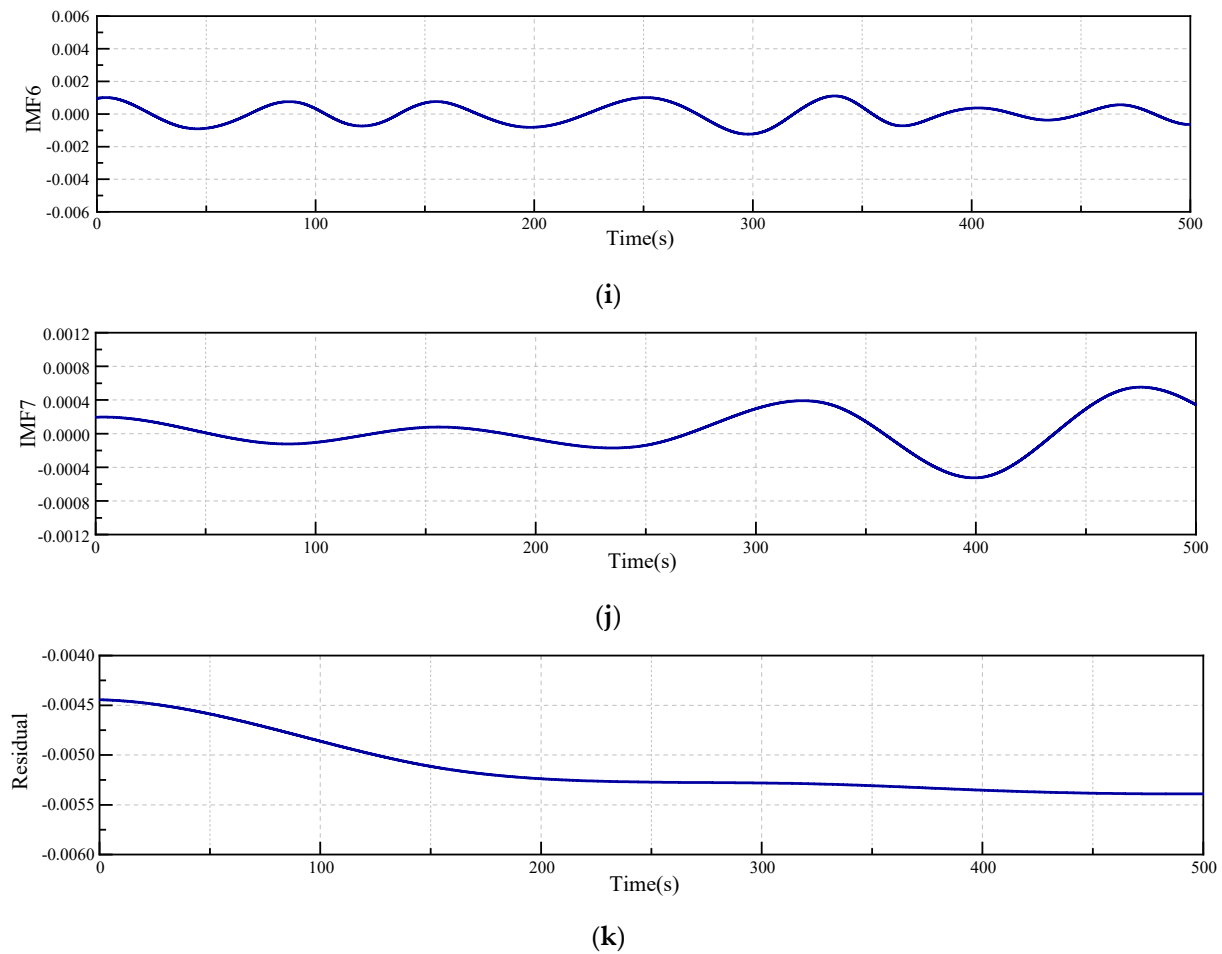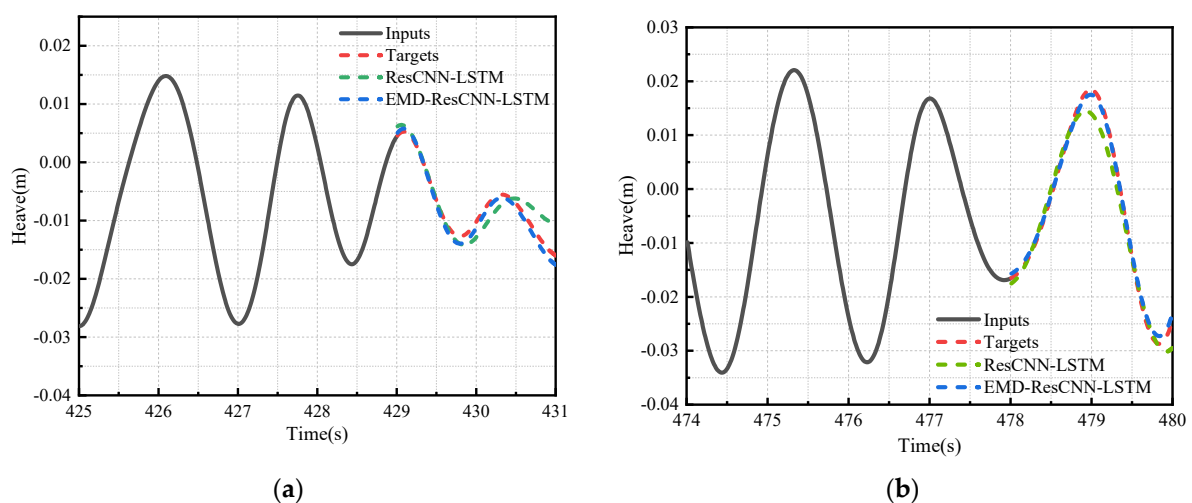
(**a**)

(**b**)

(**c**)

Figure 17. *Cont.*

(**d**)

(**e**)

(**f**)

(**g**)

(**h**)

Figure 17. *Cont.*
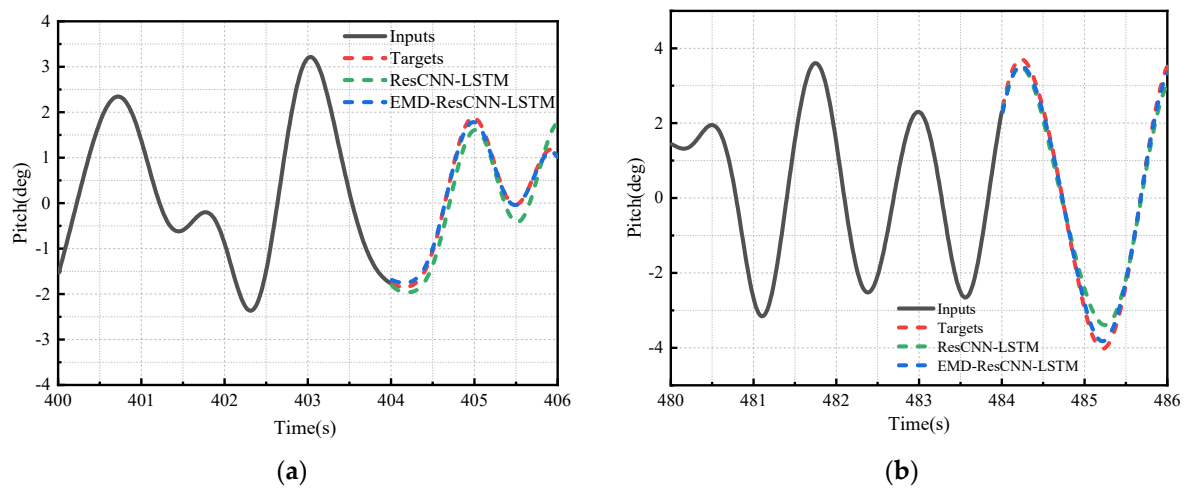
(**i**)

(**j**)

(**k**)

Figure 17. Empirical mode decomposition results of heave motion in condition one. (**a**) Input signal (0−250 s), (**b**) input signal (250−500 s), (**c**) IMF1 (0−250 s), (**d**) IMF1 (250−500 s), (**e**) IMF2 (0−500 s), (**f**) IMF3 (0−500 s), (**g**) IMF4 (0−500 s), (**h**) IMF5 (0−500 s), (**i**) IMF6 (0−500 s), (**j**) IMF7 (0−500 s), and (**k**) residual (0−500 s).

(**a**)

(**b**)

Figure 18. Single sample from heave test set of operational condition one. (**a**) 425−431 s; (**b**) 474−480 s.
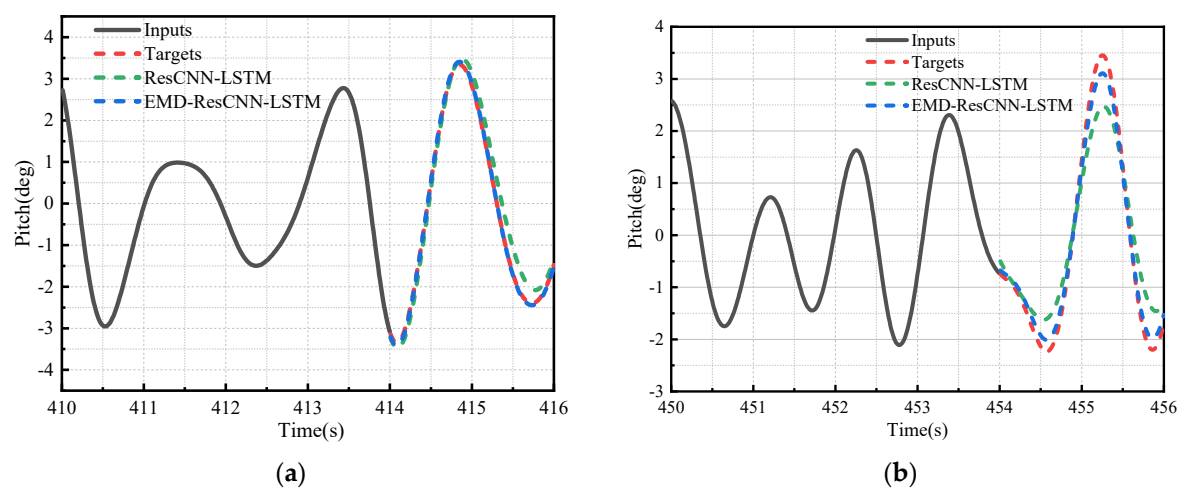
Figure 19. Single sample from pitch test set of operational condition one. (**a**) 400−406 s; (**b**) 480−486 s.
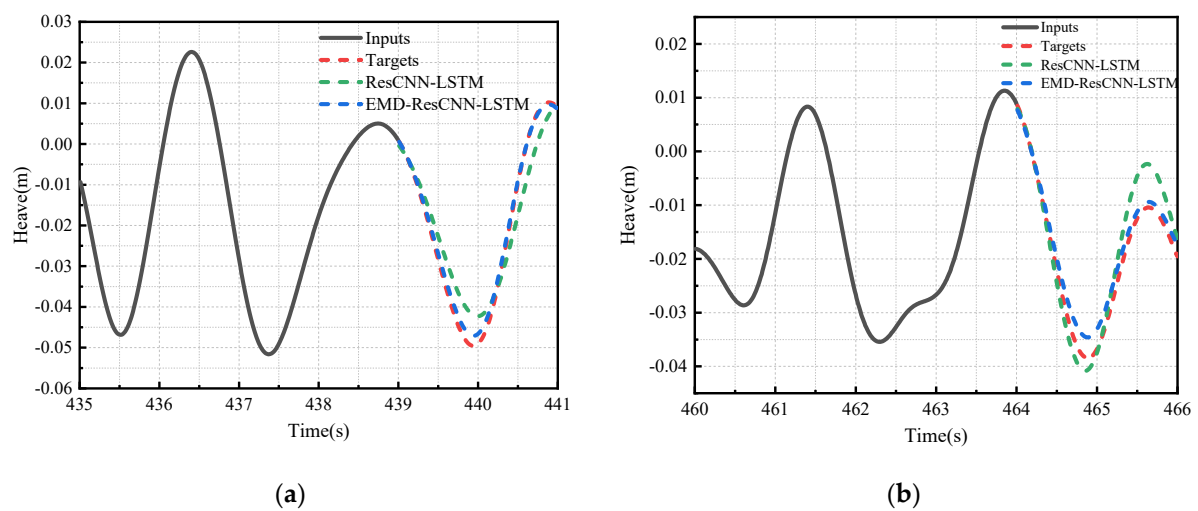
Figure 20. Single sample from heave test set of operational condition two. (**a**) 435−441 s; (**b**) 460−466 s.

Figure 21. Single sample from pitch test set of operational condition two. (**a**) 410−416 s; (**b**) 450−456 s.

Compared to the ResCNN-LSTM model, the EMD-ResCNN-LSTM model exhibits better performance in predicting peak and trough values, with results closely matching actual values and showing a smaller error range. By incorporating the EMD algorithm,

the model gains a more comprehensive understanding of signal characteristics, demonstrating a high capability to capture instantaneous frequencies for heave and pitch motions under different wave incident angles. This enhanced ability allows the model to uncover underlying patterns and information within the data, approximating an overall probability distribution model. Leveraging this approximate distribution through deductive reasoning, the model can derive potentially accurate future predictions, thus enhancing its predictive accuracy and highlighting its superiority.

Subsequently, the performance evaluation metrics of R^2, MSE, and MAPE were used to conduct an error analysis of both models. The R^2 computation results of the EMD-ResCNN-LSTM model were compared with the R^2 results of the ResCNN-LSTM model from Section 2.2, as illustrated in Figures 22 and 23.
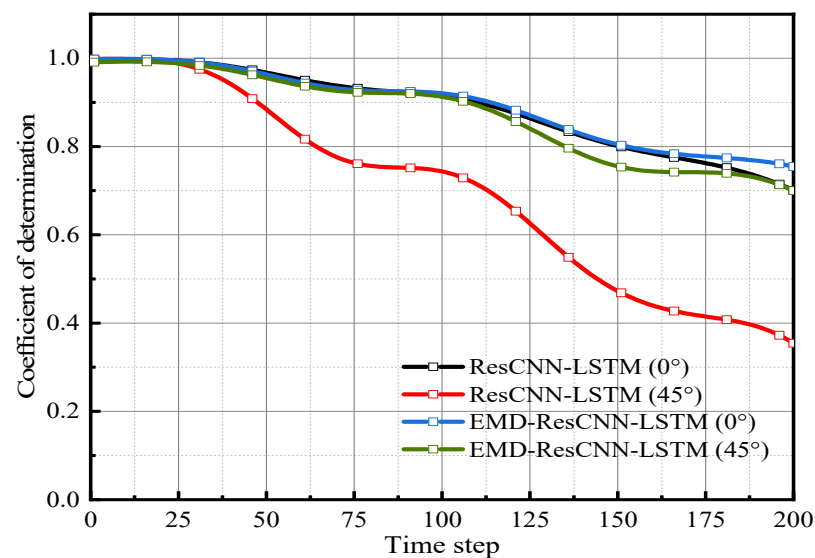

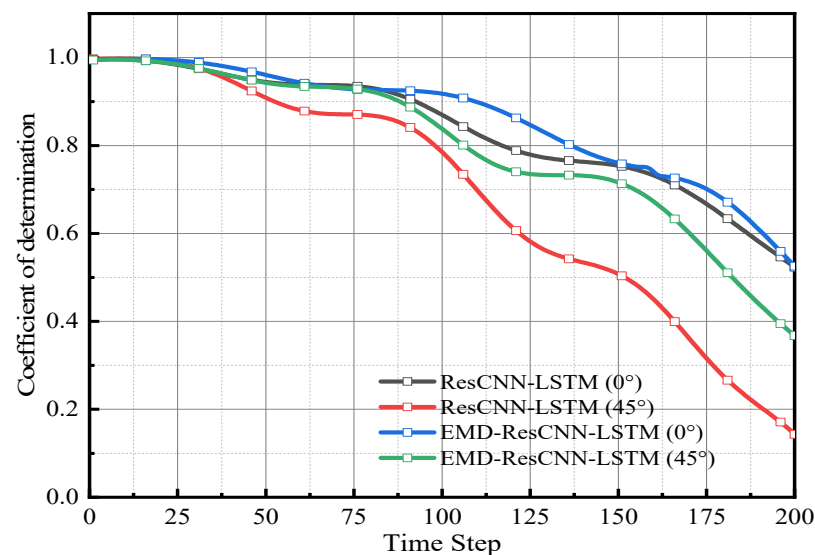**Figure 22.** Heave R^2 comparison diagram.

Figure 23. Pitch R^2 comparison diagram.

Figure 22 shows that the EMD-ResCNN-LSTM model's R^2 values exceed those of the ResCNN-LSTM model for all predicted time steps, regardless of wave incident angle (0 or 45°). The EMD-ResCNN-LSTM model demonstrates superior predictive performance, effectively addressing the shortcomings of the ResCNN-LSTM model and reducing discrepancies in predicting heave motion of offshore platforms under different wave incident

angles. The results illustrate a significant decrease in the variability of R^2 values for heave motion predictions across different wave incident angles after undergoing processing with the EMD-ResCNN-LSTM model. Notably, there is a substantial improvement in the forecast accuracy of heave motion, with R^2 values consistently exceeding 0.7 throughout the prediction time steps, particularly evident at a 45° wave incident angle.

Figure 23 compares the R^2 performance for roll motion predictions. The results demonstrate that the EMD-ResCNN-LSTM model consistently outperforms the ResCNN-LSTM model in terms of R^2 values throughout the prediction time series, indicating higher predictive accuracy. Additionally, the model effectively minimizes prediction outcome discrepancies across different wave incident angles, thereby enhancing roll motion predictive quality over the entire forecasting period. Particularly noteworthy is the performance at a 45° wave incident angle, where the R^2 values predominantly exceed 0.4, representing significant advancement over previous models.

MSE assesses average output data deviation, while MAPE evaluates the overall performance of the predicted wave height sequence. These metrics offer distinct evaluation frameworks: MSE from a two-dimensional data plane perspective and MAPE from a three-dimensional data space, providing a more comprehensive evaluation of the model's predictive capacity. This distinction is elaborated in Table 5.

Table 5. Comparison of MSE and MAPE.

	ResCNN-LSTM		EMD-ResCNN-LSTM	
	MSE	**MAPE**	**MSE**	**MAPE**
Heave (0°)	4.00×10^{-5}	0.21	3.55×10^{-5}	0.19
Heave (45°)	6.99×10^{-5}	0.38	4.25×10^{-5}	0.23
Pitch (0°)	5.23×10^{-5}	0.26	5.15×10^{-5}	0.25
Pitch (45°)	1.01×10^{-4}	0.72	7.63×10^{-5}	0.52

The MSE data in Table 5 demonstrate that the EMD-ResCNN-LSTM model consistently outperforms the ResCNN-LSTM model under identical operating conditions. This suggests inherent limitations in using the ResCNN-LSTM model directly for predictions. The motion response data comprise intricate frequency features that fluctuate substantially with varying wave incident angles, complicating the extraction of pertinent information. However, by integrating the EMD algorithm, the intricate original signal can be decomposed into components with distinct frequency characteristics, enabling more precise capture of transient frequency changes and reducing noise interference. Similarly, the MAPE values show that the EMD-ResCNN-LSTM model consistently exhibits lower values compared to the ResCNN-LSTM model under identical operating conditions. These results demonstrate that the EMD-integrated model performs well in terms of both MSE and MAPE. The mutual validation between these metrics indirectly confirms the accuracy of the R^2 values.

In conclusion, this section rigorously assesses the efficacy of integrating the EMD algorithm using three distinct dimensions of metrics. The incorporation of the EMD algorithm effectively mitigates the non-stationarity and nonlinearity present in the raw data, resulting in a remarkable enhancement in forecasting accuracy. This improvement is consistently evident throughout the entire forecasting horizon, elevating the model's performance to a higher standard and bolstering its applicability in real-world engineering settings.

5. Conclusions

This article introduces an innovative neural network-based predictive model for forecasting offshore platform motion response, designed to adapt to various sea state conditions. Through comprehensive analysis of evaluation metrics and predictive outcomes, the model's accuracy is thoroughly evaluated. This study reveals that integrating the empirical mode decomposition algorithm into the residual convolutional neural network and Long Short-Term Memory networks to form the EMD-ResCNN-LSTM model

significantly enhances predictive performance across different wave incident angles. The coefficient of determination remained above 0.5 throughout the time steps, with both mean squared error and Mean Absolute Percentage Error indicating satisfactory results. This advancement enables more precise capture of crucial motion characteristics in predicting offshore platform motion response under complex sea state conditions, resulting in improved prediction reliability and accuracy. The model has currently been analyzed only for specific wave heights and wave direction angles. Further validation is necessary to assess its applicability under more complex conditions involving the combined effects of wind, waves, and currents, as well as in real-world maritime settings. Moreover, the accuracy and stability of the model's predictions over longer time scales also require additional verification. Future research could expand upon this foundation to investigate offshore platform motion behavior precision and reliability across a broader spectrum of maritime conditions and over an extended temporal horizon.

The research outcomes provide robust technical support for the safe offshore platforms' operation and efficient marine engineering management. They enable preemptive hazard identification to safeguard lives and property while optimizing operational strategies to minimize unnecessary resource consumption. This integrated approach ensures safety while achieving cost savings, thus meeting dual objectives of security and efficiency enhancement. Furthermore, it offers new perspectives and methodologies for deeper understanding and prediction of the marine environment.

References

1. Cheng, X.; Li, G.; Skulstad, R.; Major, P.; Chen, S.; Hildre, H.P.; Zhang, H. Data-driven uncertainty and sensitivity analysis for ship motion modeling in offshore operations. *Ocean Eng.* **2019**, *179*, 261–272. [CrossRef]
2. Lee, J.-H.; Lee, J.; Kim, Y.; Ahn, Y. Prediction of wave-induced ship motions based on integrated neural network system and spatiotemporal wave-field data. *Phys. Fluids* **2023**, *35*, 097127. [CrossRef]
3. Chen, C.-Z.; Zou, Z.-J.; Zou, L.; Zou, M.; Kou, J.-Q. Time series prediction of ship course keeping in waves using higher order dynamic mode decomposition. *Phys. Fluids* **2023**, *35*, 097139. [CrossRef]
4. Elkhrachy, I.; Alhamami, A.; Alyami, S.H.; Alviz-Meza, A. Novel Ocean Wave Height and Energy Spectrum Forecasting Approaches: An Application of Semi-Analytical and Machine Learning Models. *Water* **2023**, *15*, 3254. [CrossRef]
5. Heydarizad, M.; Gimeno, L.; Minaei, M.; Gharehghouni, M.S. Stable Isotope Signatures in Tehran's Precipitation: Insights from Artificial Neural Networks, Stepwise Regression, Wavelet Coherence, and Ensemble Machine Learning Approaches. *Water* **2023**, *15*, 2357. [CrossRef]
6. Zhao, J.; Zhao, Y.; Zou, L. A fully adaptive time–frequency coupling model using self-attention mechanism based on deep operator network for very short-term forecasting of ship motion. *Phys. Fluids* **2024**, *36*, 102119. [CrossRef]
7. Li, C.; Liang, B.; Yuan, P.; Zhang, Q.; Liu, Y.; Liu, B.; Zhao, M. Fast prediction of propeller dynamic wake based on deep learning. *Phys. Fluids* **2024**, *36*, 085133. [CrossRef]
8. Guo, X.; Jin, X.; Jin, S. Shallow Water Bathymetry Mapping from ICESat-2 and Sentinel-2 Based on BP Neural Network Model. *Water* **2022**, *14*, 3862. [CrossRef]
9. Vicens-Miquel, M.; Tissot, P.E.; Medrano, F.A. Exploring Deep Learning Methods for Short-Term Tide Gauge Water Level Predictions. *Water* **2024**, *16*, 2886. [CrossRef]
10. Liu, B.; Zhang, Y.; Pan, D.; Xu, X.; Cai, T. Amphibious vehicle's resistance optimization through neural networks and genetic algorithms. *Phys. Fluids* **2024**, *36*, 065129. [CrossRef]
11. Deo, I.K.; Jaiman, R. Predicting waves in fluids with deep neural network. *Phys. Fluids* **2022**, *34*, 067108. [CrossRef]

12. Jiao, Y.; Li, G.; Zhao, P.; Chen, X.; Cao, Y.; Liu, G.; Wu, L.; Xu, X.; Fu, D.; Xin, R.; et al. Construction of Sea Surface Temperature Forecasting Model for Bohai Sea and Yellow Sea Coastal Stations Based on Long Short-Time Memory Neural Network. *Water* **2024**, *16*, 2307. [CrossRef]

13. Zhao, X.; Wang, H.; Bai, M.; Xu, Y.; Dong, S.; Rao, H.; Ming, W. A Comprehensive Review of Methods for Hydrological Forecasting Based on Deep Learning. *Water* **2024**, *16*, 1407. [CrossRef]

14. Ouyang, Z.; Gao, Y.; Zhang, X.; Wu, X.; Zhang, D. Significant Wave Height Forecasting Based on EMD-TimesNet Networks. *J. Mar. Sci. Eng.* **2024**, *12*, 536. [CrossRef]

15. Hou, X.; Xia, S. Short-Term Prediction of Ship Roll Motion in Waves Based on Convolutional Neural Network. *J. Mar. Sci. Eng.* **2024**, *12*, 102. [CrossRef]

16. Yang, B. Research on Ultra-Short-Term Prediction of Ship Motion Attitude Based on Deep Learning. Master's Thesis, Jiangsu University of Science and Technology, Zhenjiang, China, 2023. [CrossRef]

17. Fu, W. Research on Rapid Prediction of Damaged Ship Motion in Beam Waves Based on Machine Learning. Master's Thesis, Wuhan University of Technology, Wuhan, China, 2022. [CrossRef]

18. Duan, S. Research on Ship Motion Response Prediction and Wave Inversion Based on Deep Learning. Master's Thesis, Harbin Engineering University, Harbin, China, 2021. [CrossRef]

19. Wang, K.; Li, G. Application of DRNN Neural Network in Time Series Forecasting of Ship Roll Motion. *J. Harbin Eng. Univ.* **1997**, *1*, 41–47.

20. Xu, P.; Jin, H.; Wang, K.; Yan, L. A Novel Real-Time Prediction Method for Ship Roll Motion. *China Shipbuild.* **2002**, *1*, 72–76.

21. Goodfellow, I.; Bengio, Y.; Courville, A. *Deep Learning*; MIT Press: Cambridge, MA, USA, 2016.

22. Hochreiter, S.; Schmidhuber, J. Long short-term memory. *Neural Comput.* **1997**, *9*, 1735–1780. [CrossRef] [PubMed]

23. Graves, A. Supervised Sequence Labelling with Recurrent Neural Networks. Ph.D. Thesis, Technical University of Munich, Munich, Germany, 2008.

24. Chen, Z.; Wang, Z.; Cui, H.; Li, S. Visualization research on ship attitude estimation based on deep learning. *J. Huazhong Univ. Sci. Technol. (Nat. Sci. Ed.)* **2024**, 1–6. [CrossRef]

25. Hou, H.; Wu, W.; Wei, R.; He, H.; Wang, L.; Li, Z.; Lin, X. CNN-LSTM-XGBoost typhoon rainstorm electric power meteorological hybrid prediction model based on attention mechanism. *Smart Power* **2024**, *52*, 96–102. [CrossRef]

26. Zhu, Y.; Wu, G.; Liang, Y.; Ma, Y.; Wu, J. Classification of Distribution Network Planning Documents Based on LSTM Neural Network. *Procedia Comput. Sci.* **2023**, *228*, 914–919. [CrossRef]

27. Wei, Q.; Li, X.; Li, X.; Lu, W. Ultra-Short-Term Forecasting of Semi-Submersible Platform Motion Based on EMD-LSTM Model. *Ocean Eng.* **2021**, *39*, 29–37. [CrossRef]

28. Tian, J.; Wu, K. Bearing fault diagnosis based on improved one-dimensional convolutional neural network. *Mech. Eng. Autom.* **2024**, *5*, 158–159+162.

29. Xu, Y.; Wei, J.; Wei, C.; Yang, F. A High-Frequency Ground Wave Radar Ocean Current Direction Correction Method Based on CNN-LSTM. *J. Trop. Oceanogr.* **2024**, 1–11. Available online: http://kns.cnki.net/kcms/detail/44.1500.P.20241104.1543.005.html (accessed on 25 November 2024).

30. Zhang, S. *Research on Instantaneous Prediction Algorithm of Wave Height Based on Neural Network*; Jiangsu University of Science and Technology: Zhenjiang, China, 2024. [CrossRef]

31. Zhang, Y.; Zhao, J.; Quan, M. Prediction Method of Effluent Ammonia Nitrogen Concentration Using Long Short-Term Memory Network Based on Convolutional Layer Attention Mechanism. *J. Chem. Eng.* **2024**, 1–18. Available online: http://kns.cnki.net/kcms/detail/11.1946.TQ.20240725.1432.002.html (accessed on 25 November 2024).

32. Diao, F.; Liu, T.; Likeufack Mdemaya, F.A.; Xu, G. Study on the Prediction of Motion Response of Offshore Platforms Based on ResCNN-LSTM. *J. Mar. Sci. Eng.* **2024**, *12*, 1869. [CrossRef]

33. Yang, J. Research on Dynamic Tension Prediction Method of Single-Point Mooring System Based on Deep Learning. Master's Thesis, Harbin Engineering University, Harbin, China, 2022. [CrossRef]

34. Lo, W.; Wang, W.-J.; Chen, H.-Y.; Lee, J.-W.; Vojinovic, Z. Feasibility Study Regarding the Use of a Conformer Model for Rainfall-Runoff Modeling. *Water* **2024**, *16*, 3125. [CrossRef]

35. Wang, T.; Ding, L.; Zhang, D.; Chen, J. A Hybrid Model Combined Deep Neural Network and Beluga Whale Optimizer for China Urban Dissolved Oxygen Concentration Forecasting. *Water* **2024**, *16*, 2966. [CrossRef]

36. Niu, G. Influence of Float Shape on the Motion Performance of Offshore Satellite Launch Platforms. Master's Thesis, Jiangsu University of Science and Technology, Zhenjiang, China, 2021. [CrossRef]

37. Yue, X. Application Research of Empirical Mode Decomposition Algorithm. Master's Thesis, Xidian University, Xi'an, China, 2013.

38. Li, G.; Han, Y.; Yang, H. A novel approach for underwater acoustic signal denoising based on improved time-variant filtered empirical mode decomposition and weighted fusion filtering. *Ocean. Eng.* **2024**, *313 Pt 3*, 119550, ISSN 0029-8018. [CrossRef]

39. Boudraa, A.-O.; Khaldi, K.; Chonavel, T.; Hadj-Alouane, M.T.; Komaty, A. Audio coding via EMD. *Digit. Signal Process.* **2020**, *104*, 102770. [CrossRef]

40. Chen, Q.; Wen, D.; Li, X.; Chen, D.; Lv, H.; Zhang, J.; Gao, P. Empirical mode decomposition based long short-term memory neural network forecasting model for the short-term metro passenger flow. *PLoS ONE* **2019**, *14*, e0222365. [CrossRef]